Electronic Supplementary Material (ESI) for Physical Chemistry Chemical Physics.

Supporting Information

Excited State Proton Transfer of Triplet State *p*-Nitrophenylphenol to Amine and Alcohol: A Spectroscopic and Kinetic Study

Xinghang Pan[a], Ting Han[a], Jing Long[a], Binbin Xie[b], Yong Du[c], Yanying Zhao[a,d], Xuming Zheng[a], Jiadan Xue[*a,d]

[a]*Department of Chemistry, Zhejiang Sci-Tech University, Hangzhou, 310018, China*

[b]*Zhejiang Normal University, Hangzhou Institute of Advanced Studies, Hangzhou 310018, China*

[c]*Centre for THz Research, China Jiliang University, Hangzhou, 310018, China*

[d]*Key Laboratory of Surface & Interface Science of Polymer Materials of Zhejiang Province, Zhejiang Sci-Tech University, Hangzhou, 310018, China*

Content

Figure 1S. (A) UV-Vis spectra evolution for NO_2-Bp-OH under different pH conditions in MeCN:H_2O=1:9 (v:v) solution. (B) Absorptions at 328 and 426 nm associated with NO_2-Bp-OH and its deprotonated form NO_2-Bp-O^-. 4

Figure 2S. UV-vis absorption spectra of NO_2-Bp-OH in acetonitrile containing 0.4 mM Bu_4NOH and varying percentage (v%) of methanol in the solution. 4

Figure 3S. Structures of free NO_2-Bp-O^- molecule and two types of hydrogen-bonded complexes: NO_2-Bp-$O^{-}\cdots(H_2O)_n$ (n=1~3) and $(H_2O)_n\cdots NO_2$-Bp-O^- (n=1, 2). 5

Figure 4S. Plot of pseudo first-order decay rate constants of $^3NO_2$-Bp-OH versus concentrations of ferrocene with a linear fit. 5

Figure 5S. Transient absorption spectra recorded at selected time delays upon excitation of NO_2-Bp-OH in acetonitrile with *t*-butylamine (NB) in the solution. Concentrations of NB have been depicted in the graphs. 6

Figure 6S. The kinetic curves (black) measured at 650 and 490 (480) nm in the presence of various concentrations of *t*-butylamine (NB). Fitted curves (in red) obtained with a single exponential function (650 nm) and a bi-exponential function (490 nm). The influence of laser pulse duration was also included in those with fast decay. The concentrations of NB are displayed in the corresponding graphs. 8

Figure 7S. Transient absorption spectra after excitation of NO_2-Bp-OH (0.04 mM) in acetonitrile in the presence of 18.9 mM NB under argon purged. (Inserted) the expand view of the 6.0 μs spectrum. 9

Figure 8S. Plot of pseudo first-order decay rate constants of $^3NO_2$-Bp-OH vs. concentrations of *t*-butylamine (NB) with a linear fit. 9

Figure 9S. Kinetics at 520 nm at various concentrations of NO_2-Bp-O^- in the benzophenone (4.1 mM) sensitization experiments. NO_2-Bp-O^- was produced in the presence of Bu_4NOH, and confirmed by UV-Vis spectra. A bi-exponential function was used to fit the kinetic curve so that the decay time constant could be found accurately. 10

Figure 10S. Transient absorption spectra after 355 nm excitation of NO_2-Bp-O^- (40 μM) alone in solution. NO_2-Bp-O^- was produced in the presence of Bu_4NOH, and confirmed by UV-Vis spectra. 11

Figure 11S. (A) Fluorescence spectra of NO_2-Bp-OH (40 μM) in acetonitrile containing various NB concentration. NO_2-Bp-O^- does not produce any detectable emission bands. (B) Normalized fluorescence spectra without NB and with 945 mM NB in solutions. 12

NO_2-Bp-OH has a maximum emission at 534 nm and a quantum yield of 0.004 in acetonitrile. The intensity of fluorescence decreases as NB concentration increases, and no new emission bands are observed. This observation is consistent with the finding that excitation of NO_2-Bp-O^- alone in solution does not produce detectable fluorescence. 12

Figure 12S. The decay curves (black) of $^3NO_2$-Bp-OH monitored at 650 nm in the presence of various concentrations of methanol, the proportion of which is displayed in the graph. The single exponential function (in red) was used to fit the decay kinetics and the time constants are shown in the graphs. 13

Figure 13S. Transient absorption spectra recorded at selected time delays upon excitation of NO_2-Bp-OH in acetonitrile with ethanol in the solution. The volume proportions of ethanol are displayed in the graphs. 14

Figure 14S. The decay curves (black) of $^3NO_2$-Bp-OH monitored at 650 nm in the presence of various concentrations of ethanol, the proportion of which is displayed in the graph. The single exponential function (in red) was used to fit the decay kinetics and the time constants are shown in the graphs. 15

Figure 15S. T_1 state NO_2-Bp-OH$\cdots(MeOH)_n$ (n=1~3) hydrogen-bonded complexes in acetonitrile used in the potential energy scan. 16

Table 1S. Hydrogen bond lengths and hydrogen-bonding energies of NO_2-Bp-$O^-\cdots(H_2O)_n$ (n=1~3) and $(H_2O)_n\cdots NO_2$-Bp-O^- (n=1,2) complexes predicted by DFT calculation at the level of B3LYP/6-31+G(d,p) in acetonitrile with PCM model. 17

Table 2S. Vibrational frequencies of NO_2-Bp-$O^-\cdots(H_2O)_n$ (n=1~3) and $(H_2O)_n\cdots NO_2$-Bp-O^- (n=1,2) hydrogen-bonded complex predicted by DFT calculation at the level of B3LYP/6-31+G(d,p). 18

Table 3S. Selected structural parameters of the NO_2-Bp-$O^-\cdots(H_2O)_n$ (n=1~3) and $(H_2O)_n\cdots NO_2$-Bp-O^- (n=1,2) hydrogen-bonded complex predicted by DFT calculation at the level of B3LYP/6-31+G(d,p).[a] 19

Determination of the acidity (pK_a^*) of $^3NO_2$-Bp-OH 20

References: 20

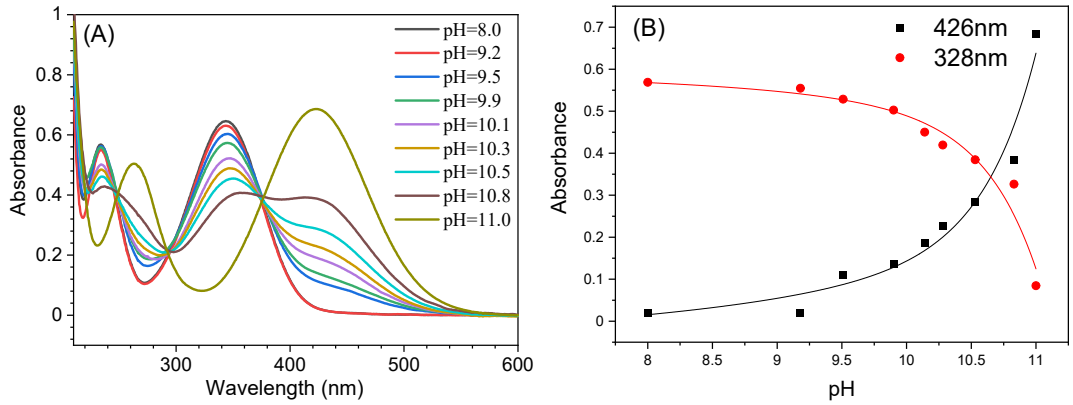

Figure 1S. (A) UV-Vis spectra evolution for NO_2-Bp-OH under different pH conditions in MeCN:H_2O=1:9 (v:v) solution. (B) Absorptions at 328 and 426 nm associated with NO_2-Bp-OH and its deprotonated form NO_2-Bp-O^-.

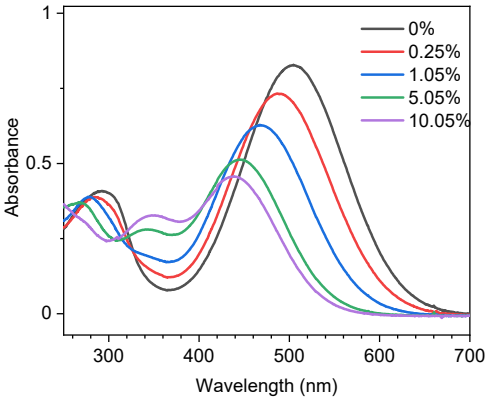

Figure 2S. UV-vis absorption spectra of NO_2-Bp-OH in acetonitrile containing 0.4 mM Bu_4NOH and varying percentage (v%) of methanol in the solution.

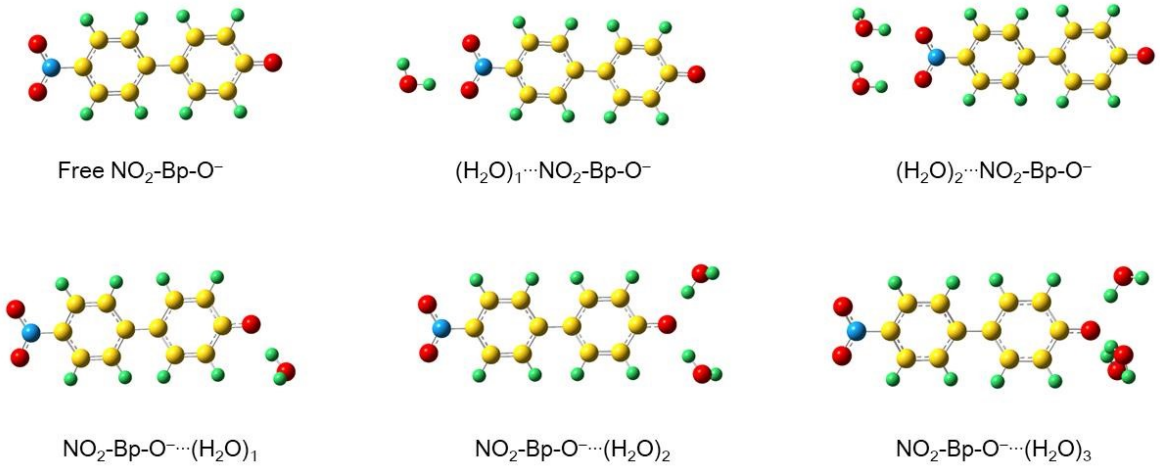

Figure 3S. Structures of free NO_2-Bp-O^- molecule and two types of hydrogen-bonded complexes: NO_2-Bp-$O^-\cdots(H_2O)_n$ (n=1~3) and $(H_2O)_n\cdots NO_2$-Bp-O^- (n=1, 2).

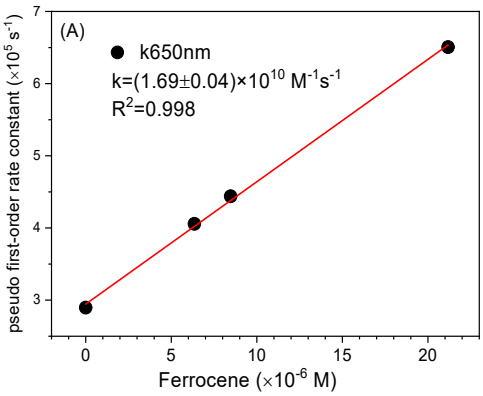

Figure 4S. Plot of pseudo first-order decay rate constants of $^3NO_2$-Bp-OH versus concentrations of ferrocene with a linear fit.

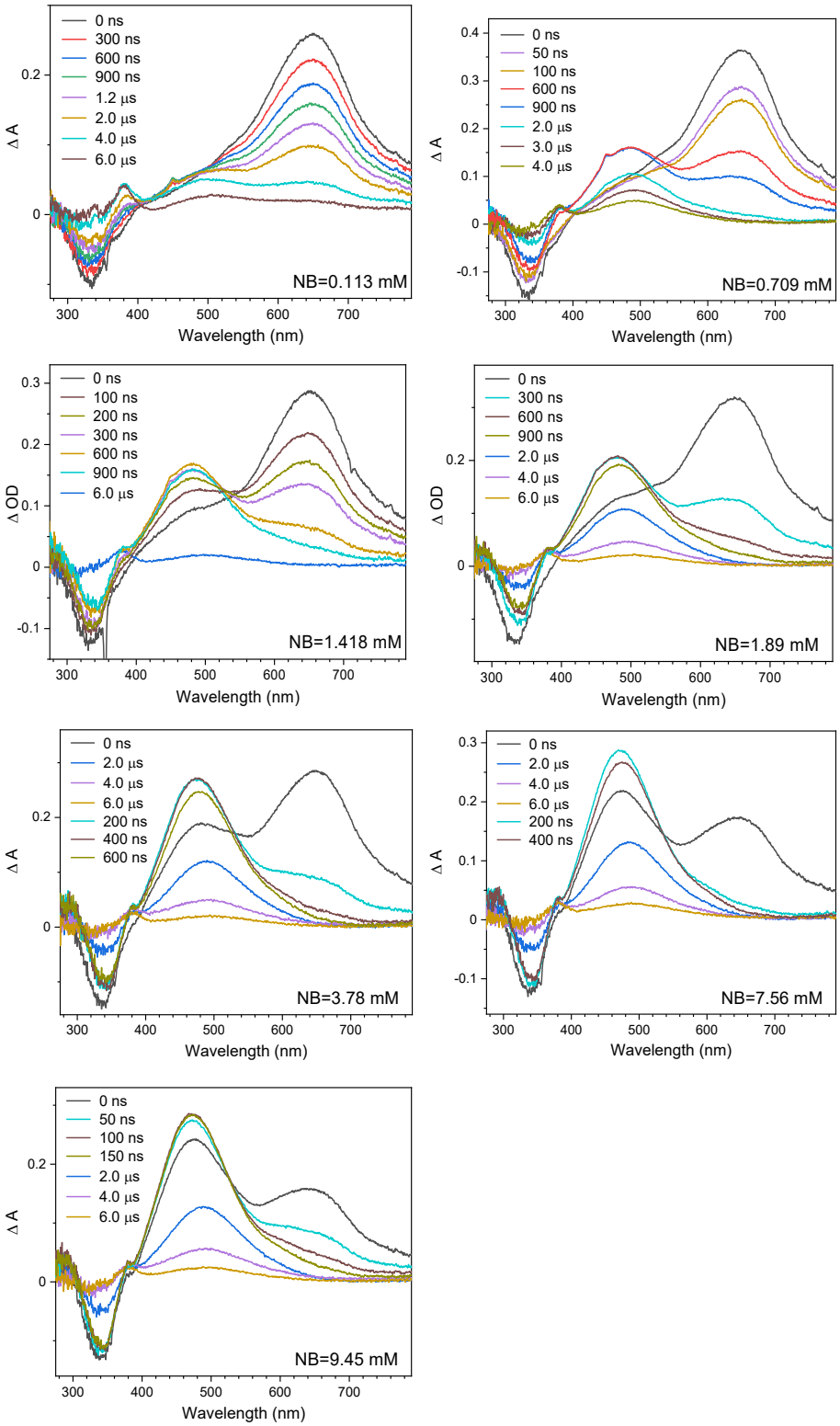

Figure 5S. Transient absorption spectra recorded at selected time delays upon excitation of NO_2-Bp-OH in acetonitrile with *t*-butylamine (NB) in the solution. Concentrations of NB have been depicted in the graphs.

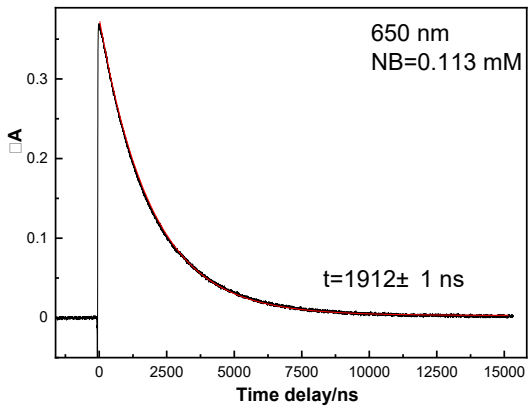
650 nm
NB=0.113 mM
t=1912± 1 ns
□A
Time delay/ns

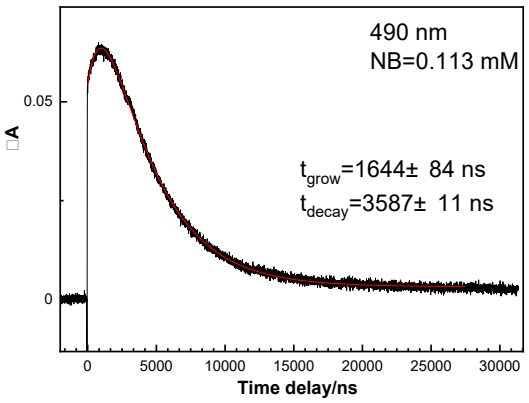
490 nm
NB=0.113 mM
t_{grow}=1644± 84 ns
t_{decay}=3587± 11 ns
□A
Time delay/ns

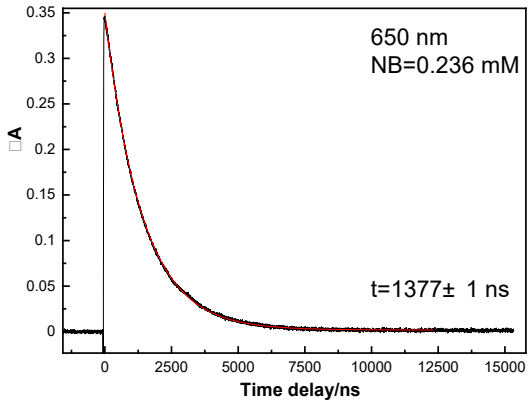
650 nm
NB=0.236 mM
t=1377± 1 ns
□A
Time delay/ns

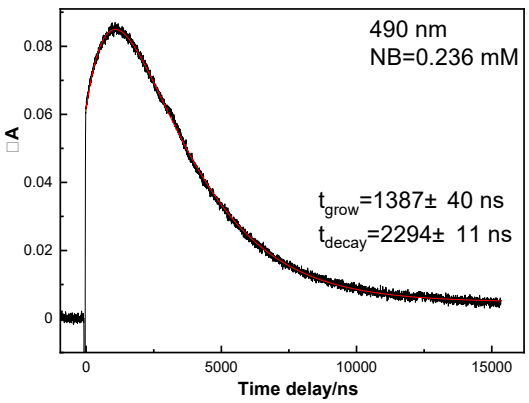
490 nm
NB=0.236 mM
t_{grow}=1387± 40 ns
t_{decay}=2294± 11 ns
□A
Time delay/ns

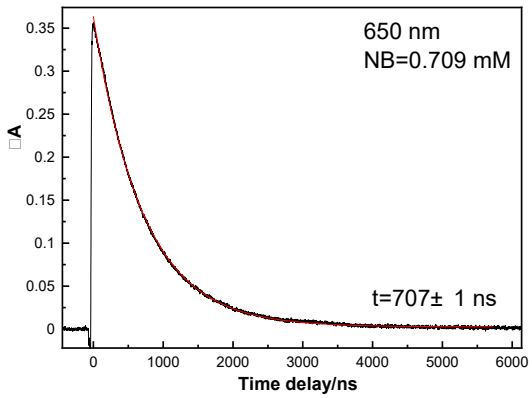
650 nm
NB=0.709 mM
t=707± 1 ns
□A
Time delay/ns

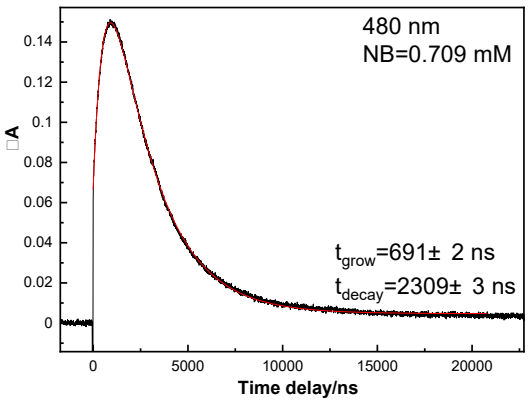
480 nm
NB=0.709 mM
t_{grow}=691± 2 ns
t_{decay}=2309± 3 ns
□A
Time delay/ns

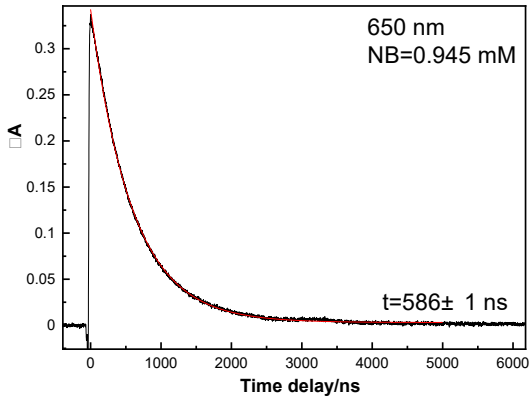
650 nm
NB=0.945 mM
t=586± 1 ns
□A
Time delay/ns

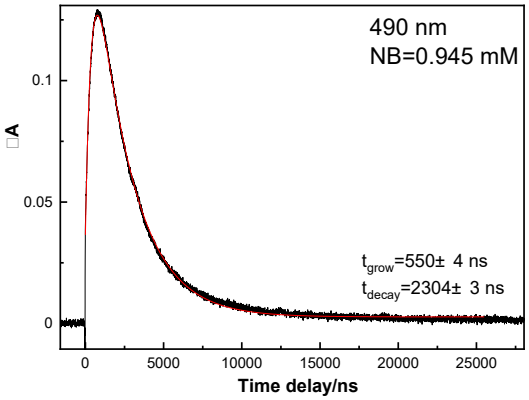
490 nm
NB=0.945 mM
t_{grow}=550± 4 ns
t_{decay}=2304± 3 ns
□A
Time delay/ns

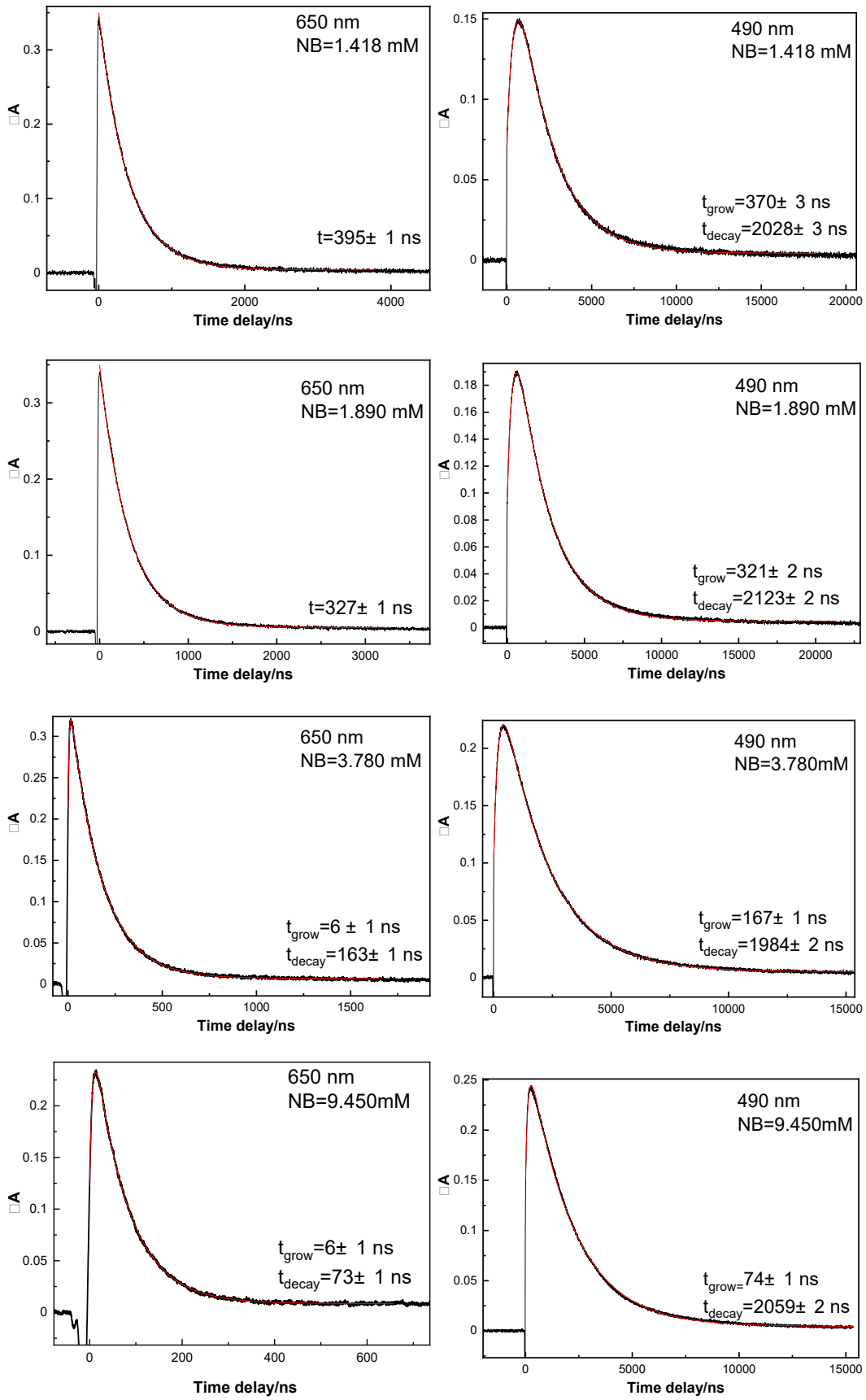

Figure 6S. The kinetic curves (black) measured at 650 and 490 (480) nm in the presence of various concentrations of *t*-butylamine (NB). Fitted curves (in red) obtained with a single exponential function (650 nm) and a bi-exponential function (490 nm). The influence of laser pulse duration was also included in those with fast decay. The concentrations of NB are displayed in the corresponding graphs.

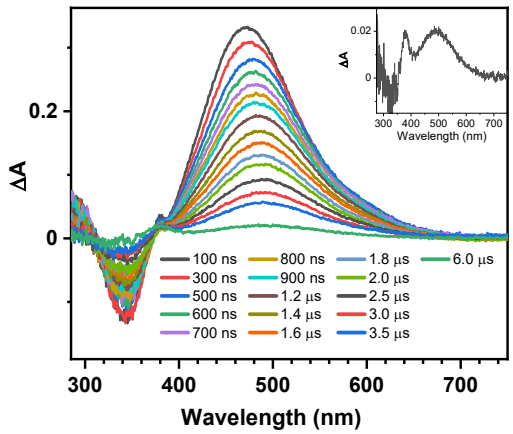

Figure 7S. Transient absorption spectra after excitation of NO_2-Bp-OH (0.04 mM) in acetonitrile in the presence of 18.9 mM NB under argon purged. (Inserted) the expand view of the 6.0 μs spectrum.

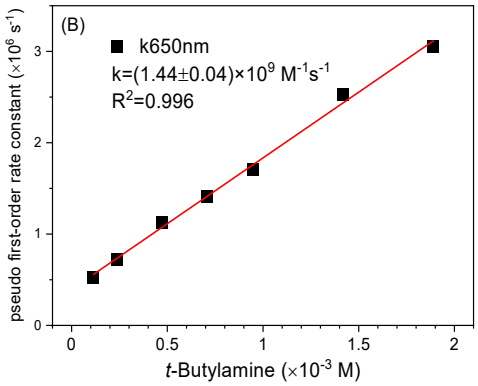

Figure 8S. Plot of pseudo first-order decay rate constants of $^3NO_2$-Bp-OH vs. concentrations of *t*-butylamine (NB) with a linear fit.

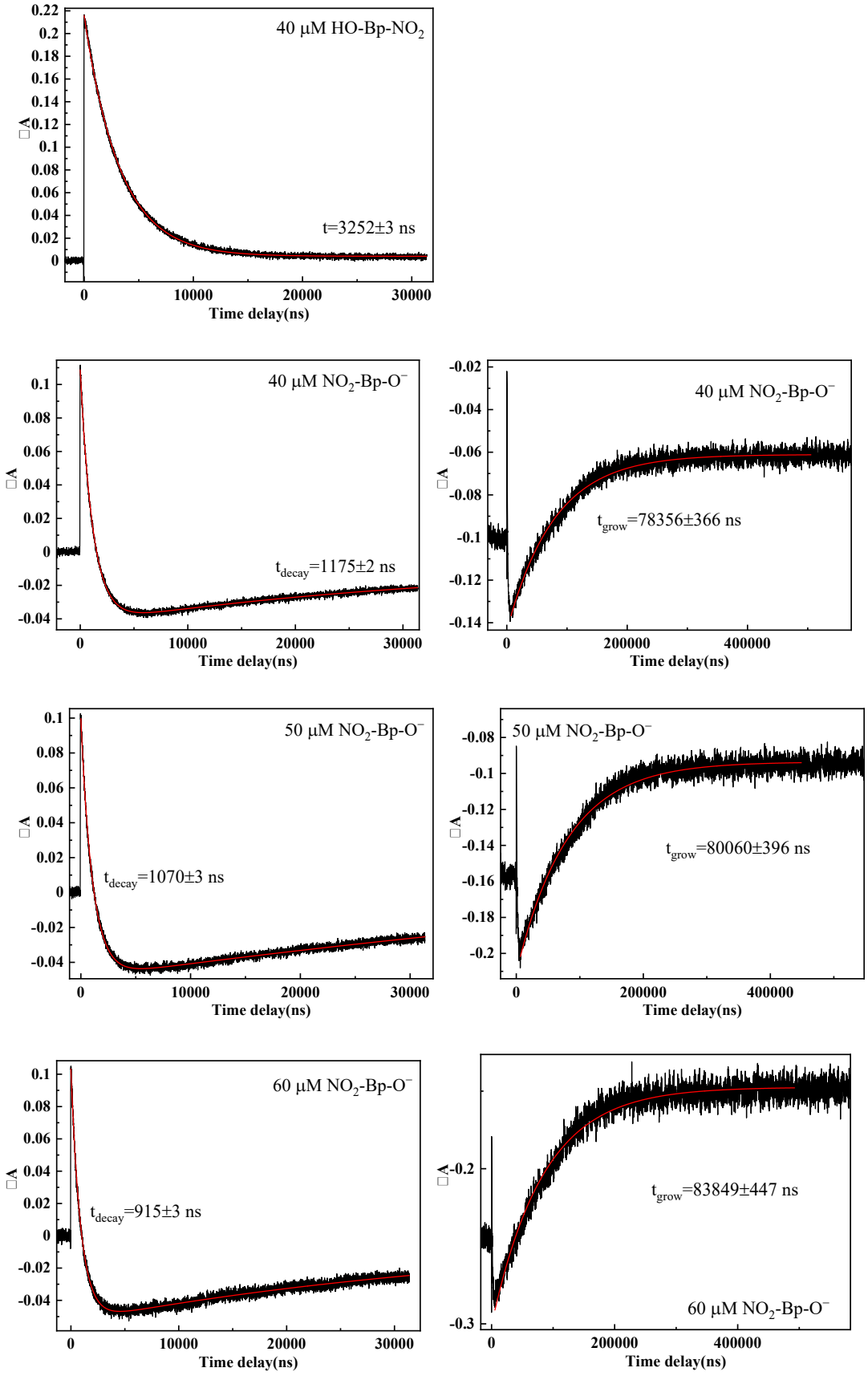

Figure 9S. Kinetics at 520 nm at various concentrations of NO_2-Bp-O^- in the benzophenone (4.1 mM) sensitization experiments. NO_2-Bp-O^- was produced in the presence of Bu_4NOH, and confirmed by UV-Vis spectra. A bi-exponential function was used to fit the kinetic curve so that the decay time constant could be found accurately.

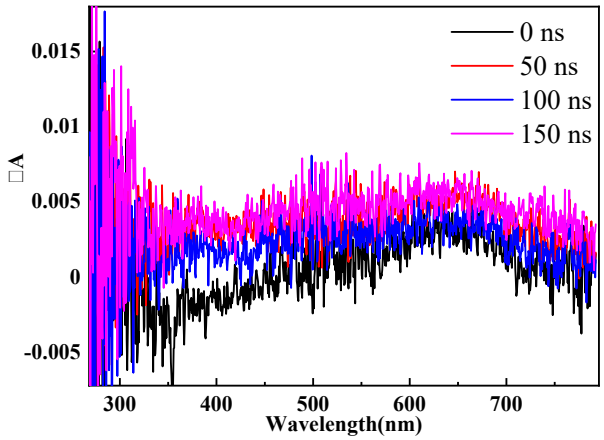

Figure 10S. Transient absorption spectra after 355 nm excitation of NO_2-Bp-O^- (40 μM) alone in solution. NO_2-Bp-O^- was produced in the presence of Bu_4NOH, and confirmed by UV-Vis spectra.

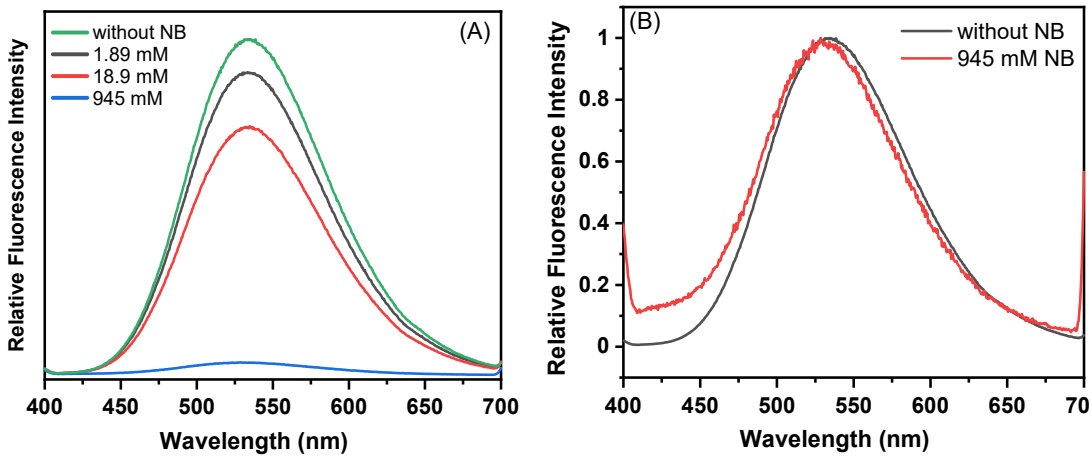

Figure 11S. (A) Fluorescence spectra of NO_2-Bp-OH (40 μM) in acetonitrile containing various NB concentration. NO_2-Bp-O^- does not produce any detectable emission bands. (B) Normalized fluorescence spectra without NB and with 945 mM NB in solutions.

NO_2-Bp-OH has a maximum emission at 534 nm and a quantum yield of 0.004 in acetonitrile. The intensity of fluorescence decreases as NB concentration increases, and no new emission bands are observed. This observation is consistent with the finding that excitation of NO_2-Bp-O^- alone in solution does not produce detectable fluorescence.

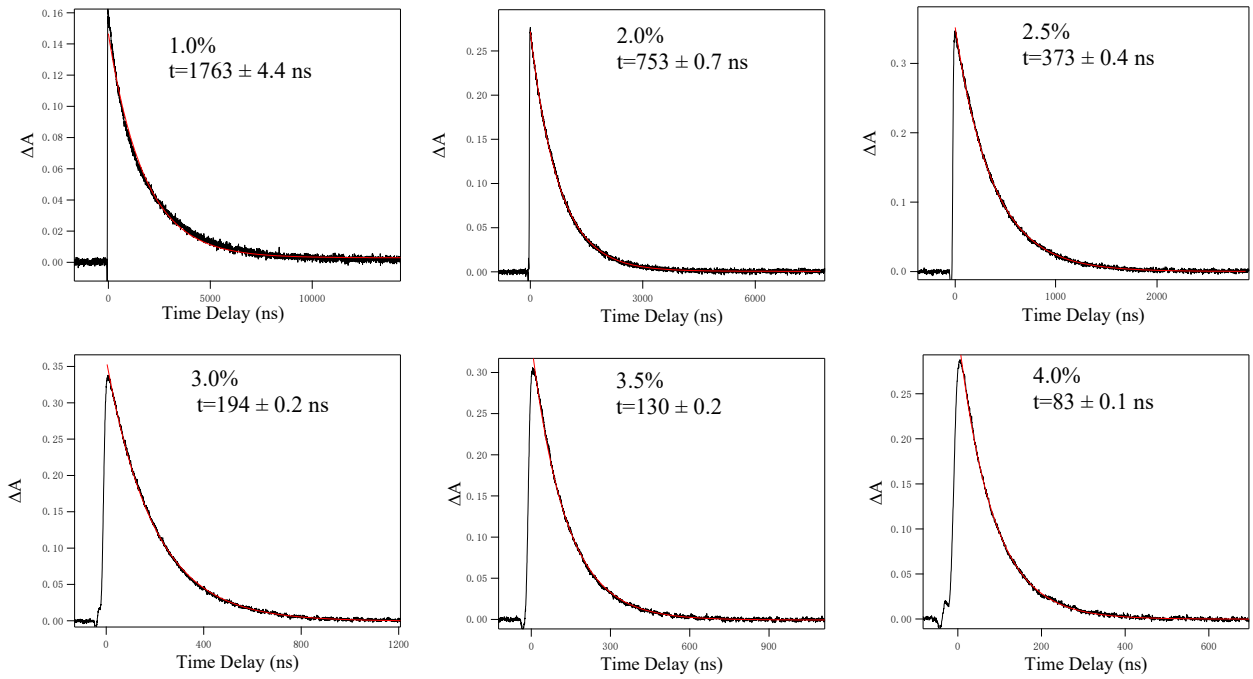

Figure 12S. The decay curves (black) of $^3NO_2$-Bp-OH monitored at 650 nm in the presence of various concentrations of methanol, the proportion of which is displayed in the graph. The single exponential function (in red) was used to fit the decay kinetics and the time constants are shown in the graphs.

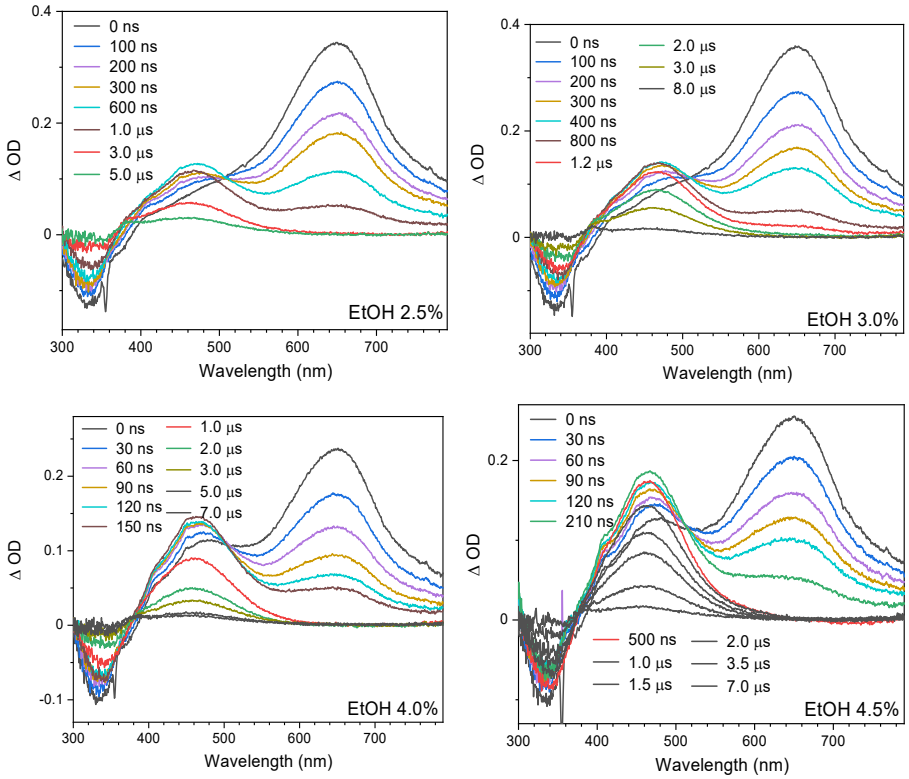

Figure 13S. Transient absorption spectra recorded at selected time delays upon excitation of NO_2-Bp-OH in acetonitrile with ethanol in the solution. The volume proportions of ethanol are displayed in the graphs.

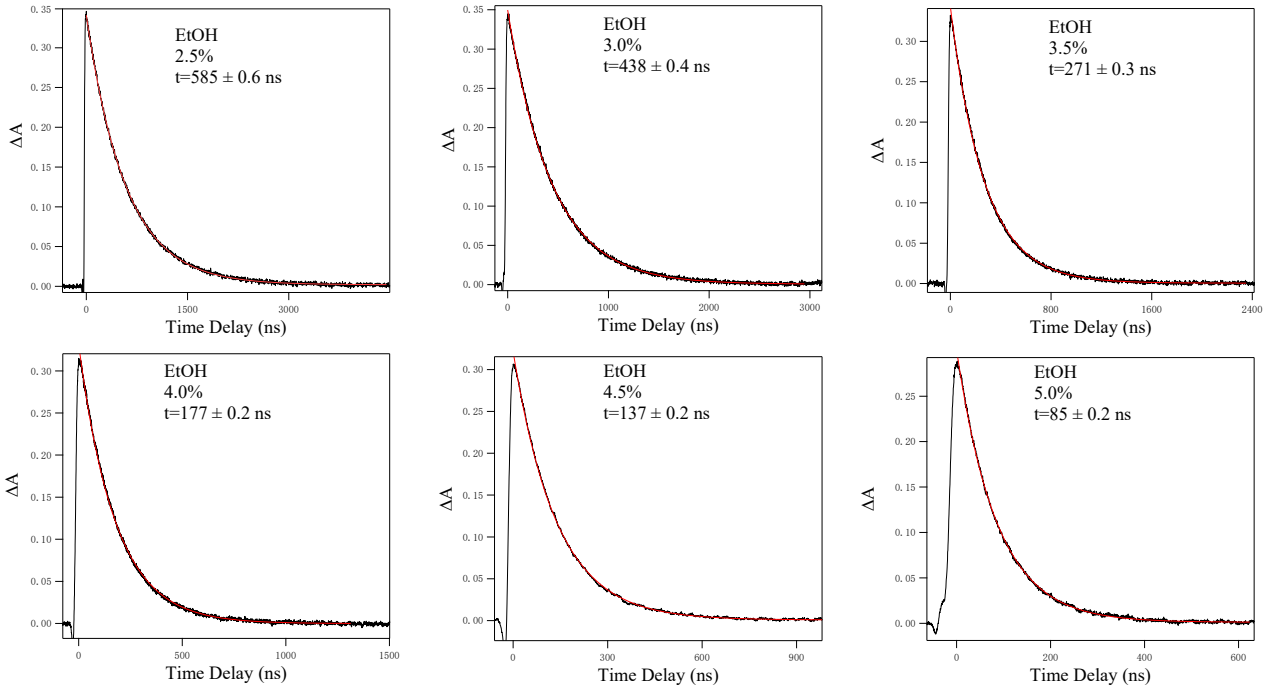

Figure 14S. The decay curves (black) of $^3NO_2$-Bp-OH monitored at 650 nm in the presence of various concentrations of ethanol, the proportion of which is displayed in the graph. The single exponential function (in red) was used to fit the decay kinetics and the time constants are shown in the graphs.

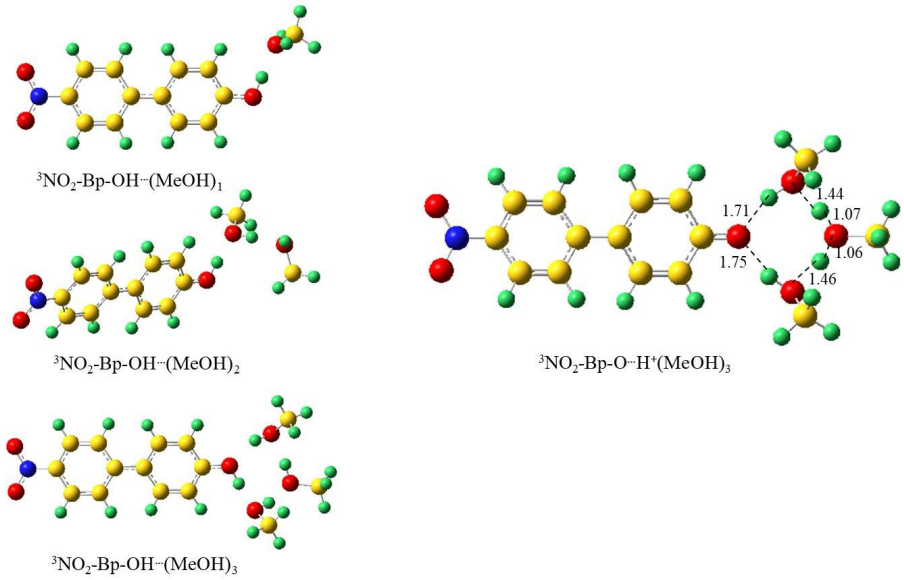

Figure 15S. T_1 state NO_2-Bp-OH···$(MeOH)_n$ (n=1~3) hydrogen-bonded complexes in acetonitrile used in the potential energy scan.

Table 1S. Hydrogen bond lengths and hydrogen-bonding energies of NO_2-Bp-$O^{-}\cdots(H_2O)_n$ (n=1~3) and $(H_2O)_n\cdots NO_2$-Bp-O^{-} (n=1,2) complexes predicted by DFT calculation at the level of B3LYP/6-31+G(d,p) in acetonitrile with PCM model.

Complex abbreviation	Hydrogen bond length (Å)	ΔH (kcal/mol)
NO_2-Bp-$O^{-}\cdots(H_2O)_1$	1.6567	6.6
NO_2-Bp-$O^{-}\cdots(H_2O)_2$	1.6833 1.6834	12.7
NO_2-Bp-$O^{-}\cdots(H_2O)_3$	1.7098 1.7303 1.7345	17.0
$(H_2O)_1\cdots NO_2$-Bp-O^{-}	1.8862	2.6
$(H_2O)_2\cdots NO_2$-Bp-O^{-}	1.8644 2.0035	6.6

Table 2S. Vibrational frequencies of NO_2-Bp-$O^-\cdots(H_2O)_n$ (n=1~3) and $(H_2O)_n\cdots NO_2$-Bp-O^- (n=1,2) hydrogen-bonded complex predicted by DFT calculation at the level of B3LYP/6-31+G(d,p).

Complex abbreviation	Calc. values (unscaled)	
	Freq. (cm^{-1})	Raman Activity
Free NO_2-Bp-O^-	1338	10218
	1601	2125
NO_2-Bp-$O^-\cdots(H_2O)_1$	1604	9224
	1335	8273
NO_2-Bp-$O^-\cdots(H_2O)_2$	1607	18327
	1332	9982
NO_2-Bp-$O^-\cdots(H_2O)_3$	1610	25302
	1330	9856
$(H_2O)_1\cdots NO_2$-Bp-O^-	1344	9748
$(H_2O)_2\cdots NO_2$-Bp-O^-	1348	10658

The hydrogen bond at the nitro group causes the (unscaled) frequency of C–C + C–N stretching from 1338 cm^{-1} in free NO_2-Bp-O^- to 1344 cm^{-1} for one water and further to 1348 cm^{-1} for two water in the $(H_2O)_n\cdots NO_2$-Bp-O^- (n=1, 2) complex.

Table 3S. Selected structural parameters of the NO_2-Bp-$O^{-}\cdots(H_2O)_n$ (n=1~3) and $(H_2O)_n\cdots NO_2$-Bp-O^{-} (n=1,2) hydrogen-bonded complex predicted by DFT calculation at the level of B3LYP/6-31+G(d,p).[a]

Bond length (Å)	Simple anion	CO-1H_2O	CO-2H_2O	CO-3H_2O	NO_2-2H_2O
C1-C2	1.425	1.422	1.420	1.417	1.428
C2-C3	1.382	1.384	1.385	1.386	1.379
C3-C4	1.406	1.404	1.403	1.402	1.411
C4-C5	1.406	1.404	1.403	1.402	1.411
C5-C6	1.382	1.384	1.385	1.386	1.379
C6-C1	1.425	1.422	1.420	1.417	1.429
C1-C7	1.456	1.461	1.465	1.470	1.449
C7-C8	1.423	1.420	1.417	1.414	1.427
C8-C9	1.380	1.383	1.385	1.388	1.377
C9-C10	1.444	1.436	1.430	1.423	1.446
C10-C11	1.444	1.436	1.430	1.423	1.446
C11-C12	1.380	1.383	1.385	1.388	1.377
C12-C7	1.423	1.419	1.417	1.414	1.427
C10-O21	1.279	1.291	1.303	1.317	1.275
C4-N22	1.428	1.434	1.439	1.444	1.411
N22-O23	1.250	1.247	1.245	1.243	1.260
N22-O24	1.250	1.247	1.245	1.243	1.255

[a]Structure geometries indicated by complex abbreviations are listed below.

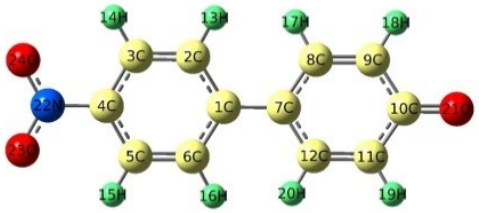

The hydrogen bond formed between the nitro group and water significantly shortens the bond lengths of C–N from 1.428 Å to 1.411 Å and C–C (bridge between two phenyl rings) from 1.456 Å to 1.449 Å. The shorter bond causes the stretching vibrations to shift to blue.

Determination of the acidity (pK_a^*) of $^3NO_2$-Bp-OH

The acid-base reaction in the triplet state of NO_2-Bp-OH can be accounted for by the following scheme, where τ_0 and τ_0' denote the lifetimes of $^3NO_2$-Bp-OH and $^3NO_2$-Bp-O$^-$ respectively, k_1 and k_2 the dissociation and protonation rate constants in the triplet state, respectively.

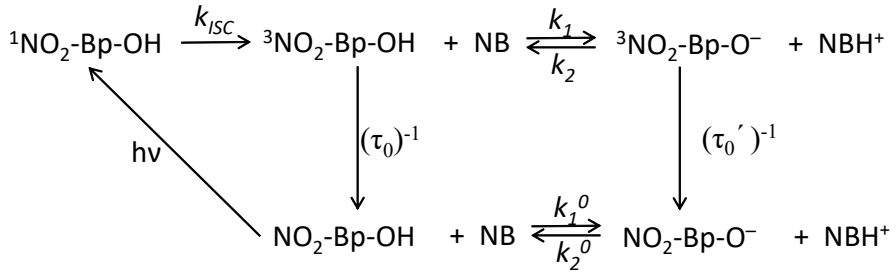

If we assume that the rates of proton transfer reactions (k_1[NB] and k_2[NBH$^+$]) in the triplet state are very fast in comparision with the triplet decay rates $(\tau_0)^{-1}$ and $(\tau_0')^{-1}$, respectively (that is, an acid-base equilibrium is established within the triplet lifetime), the following equations based on that proposed by Ware[1] can be applied to the present system. Where τ denotes the observed triplet lifetime and K_a the equilibrium constant in the triplet, which is equal to k_1/k_2.

$$(\tau^{-1} - \tau_0^{-1})^{-1} = \{(\tau_0')^{-1} - \tau_0^{-1}\}^{-1}(1 + \frac{1}{[NB]} \times \frac{1}{K_a})$$

Plot $(\tau^{-1} - \tau_0^{-1})^{-1}$ as a function of [NB]$^{-1}$as following (τ is the decay time constants at 650 nm for $^3NO_2$-Bp-OH when [NB]≥ 1.428 mM in Table 2). Fit the plot by a linear function. From the slope and intercept, the value of $K_a = \frac{intercept}{slope}$ =22 can be determined. Since the pK_a(NB)=18.1 in acetonitrile,[2] the pK_a^*($^3NO_2$-Bp-OH) can be calculated to be 16.8.

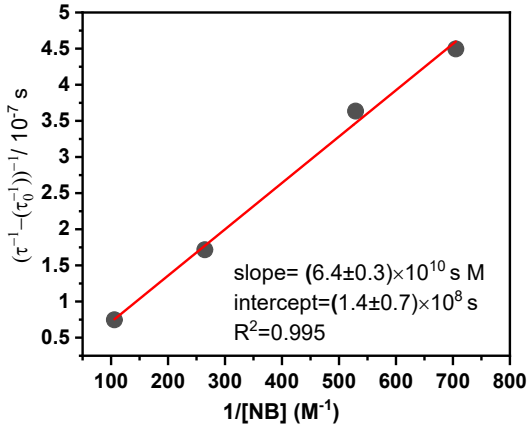

References:

(1) W. Ware, R. D. Watt and J. D. Holmes, *J. Am. Chem. Soc.*, 1974, **96**, 7853-7680.

(2) B. G. Cox, *Acid and Bases: Solvent Effects on Acid-Base Strength*, Oxford University Press, Great Clarendon Street, Oxford, OX2 6DP, United Kingdom, 2013.